ChemCatChem

The European Society Journal for Catalysis

Accepted Article

Title: Platinum-Rare Earth Alloy Electrocatalysts for the Oxygen Reduction Reaction: A Brief Overview

Authors: Carlos A. Campos-Roldán, Deborah J. Jones, Jacques Rozière, and Sara Cavaliere

Platinum-Rare Earth Alloy Electrocatalysts for the Oxygen Reduction Reaction: A Brief Overview

Carlos A. Campos-Roldán,[a] Deborah J. Jones,[a] Jacques Rozière[a] and Sara Cavaliere*[a,b]
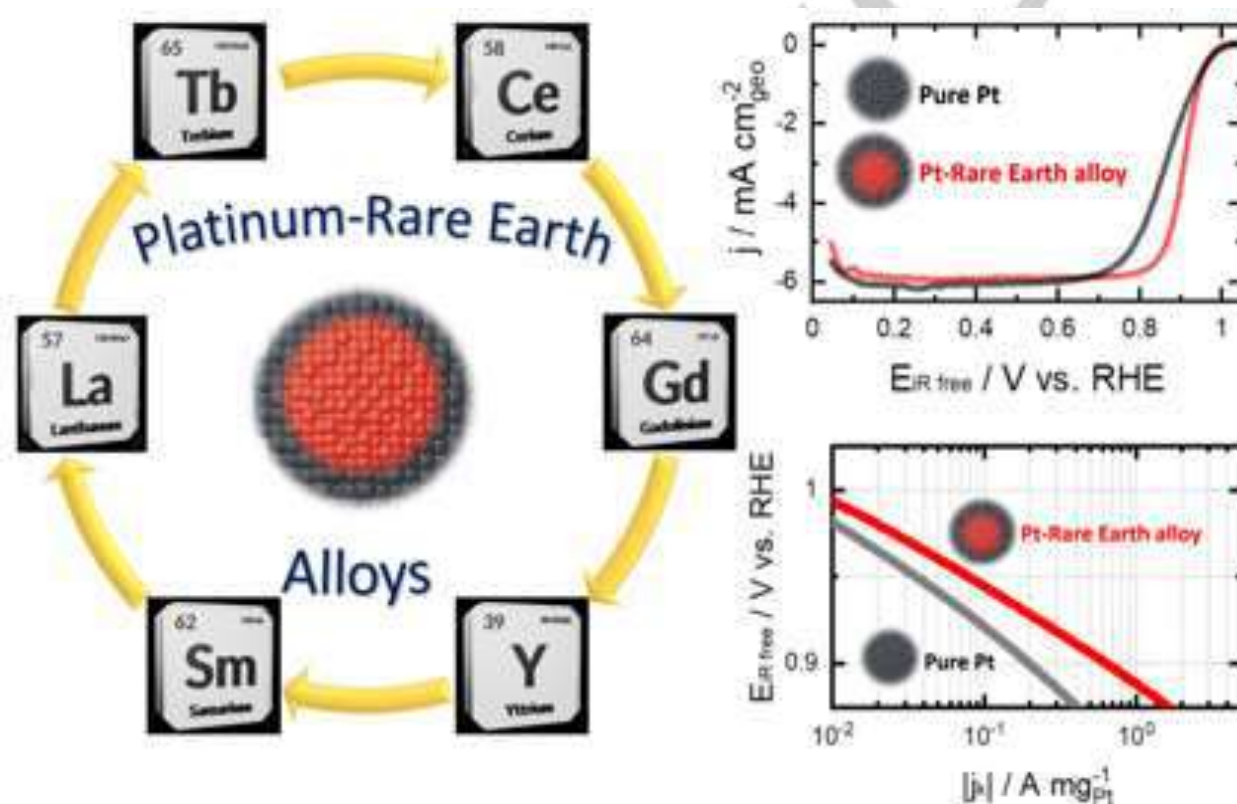
REVIEW

[a]   Dr. C.A. Campos-Roldán, Dr. D.J. Jones, Prof. J. Rozière and Prof. S. Cavaliere.
       ICGM, Univ. Montpellier, CNRS, ENSCM
       34095 Montpellier cedex 5, France
       E-mail: Sara.Cavaliere@umontpellier.fr
[b]   Prof. S. Cavaliere
       Institut Universitaire de France (IUF)
       75231 Paris cedex 05, France

Abstract: The development of highly active and long-term stable electrocatalysts for the cathode of proton-exchange membrane fuel cells (PEMFC) is a paramount requirement for high performance and durable PEMFC stacks. In this regard, alloying Pt with rare earth metals (REM) has emerged as a promising approach. This short review summarizes and discusses the most relevant advances on Pt-REM alloy electrocatalysts, from bulk polycrystalline surfaces to carbon supported nanostructures, for the oxygen reduction reaction (ORR), and their implementation in PEMFCs, and is a starting point to establish the challenges in synthesis and design and properties goals for novel Pt-REM alloys.

Jacques Rozière is Emeritus Professor of Chemistry at the University of Montpellier. Following a PhD at University of Montpellier and post-doctoral fellowships at Argonne National Laboratory, his research has encompassed structural and spectroscopic investigations of ion exchange materials and inorganic solids and the development, characterisation and implementation of materials for energy conversion.

Carlos Augusto Campos-Roldán received his PhD degree in 2020 under collaboration between ESIQIE-IPN, Mexico, and the University of Poitiers, France. His thesis was awarded in 2020 as the best electrochemistry thesis in the 13th meeting of the Mexican Section of the International Society of Electrochemistry. Currently, he is a postdoc at the University of Montpellier, France. His research interests relay on the design and understanding of nano-structured electrocatalysts for fuel cells and electrolysers.

Sara Cavaliere is Professor at the University of Montpellier, Charles Gerhardt Institute for Molecular Chemistry and Materials. She received her PhD in Chemistry and Materials Science in Versailles, France. Her work aims at developing advanced nanostructured materials to enhance performance and durability of fuel cells and electrolysers. In 2017 she was awarded the CNRS bronze medal and appointed junior member of the Institut Universitaire de France.

Deborah Jones received her Ph.D. from the University of London, King's College. She is a Director of Research at CNRS (French National Scientific Research Council) at the Charles Gerhardt Institute for Molecular Chemistry and Materials, in Montpellier, France where her research includes the development and characterisation of new materials for proton exchange membrane fuel cells and electrolysers. Fellow of the Electrochemical Society, she is a former Vice-President of the International Society of Electrochemistry.

1. Introduction

The widespread adoption of proton-exchange membrane fuel cells (PEMFCs)[1] strongly relies on a significant increase of the electrocatalyst activity for the sluggish oxygen reduction reaction (ORR),[2] and on their long-term stability in the PEMFC operating conditions.[3] Generally, the ORR is driven on the surface of Pt-based nanostructures, which is a costly and critical raw material resource.[4]

Alloying Pt with other metals is a widely used strategy to reduce the Pt loading and simultaneously enhance the ORR activity.[5] Pt-based alloys have been extensively developed, generally with 3d late transition metals such as Ni, Co, Cu, *etc.,*[2a, 2b, 5b, 6] the ORR activity of which surpass that of pure Pt.[2a] The enhanced ORR

activity of Pt-M (M = Ni, Co, Cu, *etc.*) alloys has been rationalized by the ligand effect where neighboring atoms of the alloying metal, in close vicinity, modify the electronic structure of the Pt atoms at the surface. Further, the lattice mismatch between Pt and the alloying metal induces strain effects in the crystal lattice, *e.g.,* compressive or tensile, that modulate the ORR activity[5b, 6].

Notwithstanding, leaching of the transition metal M is a major issue in such Pt-M alloys: the less noble metal segregates from the alloy and dissolves into the acidic electrolyte. As a consequence, the improved ORR activity starts to decrease as the alloyed system dissolves.[6] Furthermore, on fuel cell operation, dissolved metal ions migrate into the membrane[7] and block the proton exchange sites of the ionomer, leading to attenuation of the PEMFC performance.[8]

In another approach, advantage is taken of the partial metal dissolution process and the resulting partially de-alloyed Pt-based nanostructures achieve even higher ORR activity than conventional alloys.[2b, 9] Under PEMFC operating conditions, however, the dissolution driving force of the less noble metal is very strong. Therefore, engineering highly stable nanostructures for the PEMFC is of utmost importance.

The properties of the electrocatalysts that enhance the ORR activity might be modulated through their synthesis route by controlling parameters such as the pH of the reaction medium, alloy annealing temperature, Pt:M stoichiometry, *etc.*[6, 10] Nonetheless, the factors that will determine long-term durability are the thermodynamic alloy stability and the kinetic barriers for intermetallic diffusion.[11] In this sense, the segregation process of Pt alloys from late transition metals can be understood on the basis of their negligible alloy formation energy, ΔE_{alloy}.[11] Thus, it is proposed that the parameter which governs their stability over time is ΔE_{alloy}.[11] Taking this thermodynamic parameter as descriptor, Nørskov *et al.*[11] demonstrated that alloying Pt with rare earth metals (REM) substantially improves the long-term stability in the ORR conditions. The striking electrochemical stability of Pt-REM alloys was related to the very negative ΔE_{alloy} magnitude.[11] Likewise, it was proposed that the lattice mismatch caused by the REM atoms could control the strain effects of the alloy, therefore tuning the electrocatalytic activity and stability.[12]

In this context, the development and understanding of Pt-REM alloys represents a crucial topic for the advancement and spreading of PEMFC technology. This work aims to summarize the most representative contributions regarding the synthesis strategies of Pt-REM alloys and their application towards the ORR. First, we briefly describe the fundamental aspects of the ORR in acidic medium. Thereafter, the main outcomes on Pt-REM electrocatalyst design, from bulk polycrystalline surfaces to carbon supported nanostructures, are discussed, together with the challenges to tackle for their application in PEMFC cathodes.
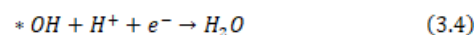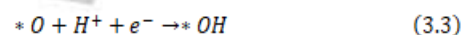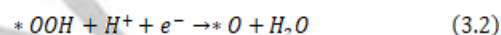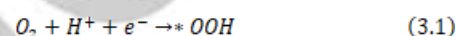
2. Oxygen Reduction Reaction

In acidic medium, the formation of water from protons and oxygen, namely the ORR, is the electrochemical process that takes place at the cathode of a PEMFC. The overall reaction proceeds as follows:

$$O_2 + 4H^+ + 4e^- \rightarrow 2H_2O \qquad E^0 = 1.23 \, V/NHE \qquad (1)$$

The ORR is generally accepted to follow either the direct four-electron pathway (Equation 1) or the two-electron pathway:

$$O_2 + 2H^+ + 2e^- \rightarrow H_2O_2 \qquad E^0 = 0.70 \, V/NHE \quad (2.1)$$

$$H_2O_2 + 2H^+ + 2e^- \rightarrow 2H_2O \qquad E^0 = 1.76 \, V/NHE \quad (2.2)$$

The complex ORR multi-electron process has been explained by two different mechanisms: associative or dissociative.[2c, 5b] Based on the associative mechanism, the ORR proceeds by a series of reactions, which involve the *OOH, *O and *OH intermediates:

$$O_2 + H^+ + e^- \rightarrow *OOH \qquad (3.1)$$

$$*OOH + H^+ + e^- \rightarrow *O + H_2O \qquad (3.2)$$

$$*O + H^+ + e^- \rightarrow *OH \qquad (3.3)$$

$$*OH + H^+ + e^- \rightarrow H_2O \qquad (3.4)$$

where * represents the species adsorbed onto the catalyst surface. In the dissociative mechanism, the oxygen is dissociated on the electrode surface before its protonation. In the fuel cell, however, the electrode performance relies on the associative mechanism.[13]

Pt-based materials are considered as the best ORR electrocatalysts in acidic medium.[14] Nevertheless, the protonation processes of the reduced O-species (see Equations 3.1-3.4) on the Pt surface present important kinetic barriers, making the ORR kinetically sluggish.[15] Density functional theory (DFT) calculations have revealed that an optimal ORR electrocatalyst should bind the oxygenated-intermediates more weakly than to a Pt (111) surface, *i.e.* 0.2 eV weaker for the *O intermediate[11, 15] or 0.1 eV weaker for the *OH intermediate.[15-16] These arguments mirror the Sabatier principle, which states that the optimal catalyst for a given reaction should bind neither too weakly nor too strongly to its intermediates.[2c] In this regard, alloying Pt with another metal is a means of tuning the electrode adsorption properties. In fact, it has been proven that compressive-strain weakens the binding energy of ORR intermediates on the Pt surface when the metal core of the alloy possesses a lattice parameter smaller than that of Pt, allowing that the Pt surface atoms will contract laterally.[17] As a consequence, there is a shifting of the Pt d-band, due to the overlap of the electronic conduction bands.[18] Therefore, the partial electron-transfer between the two metals leads to a shift in the d-band center with respect to the Fermi level,[17-19] and a resulting modification of the adsorption properties of the electrode surface.[20]

As mentioned above, Pt alloys with late transition metals experience strong degradation under the harsh ORR conditions in acid electrolyte, involving the segregation of the less-noble metal to the surface and its subsequent dissolution over time,

3

REVIEW

losing the kinetic benefit from the alloying effect.[12] Under this context, the alloy formation energy, ΔE_{alloy}, an specific thermodynamic property of alloys, has been proposed as a stability descriptor of Pt-based alloys, since this parameter represents a kinetic barrier for the alloy segregation, *c.f.* Figure 1.[12]
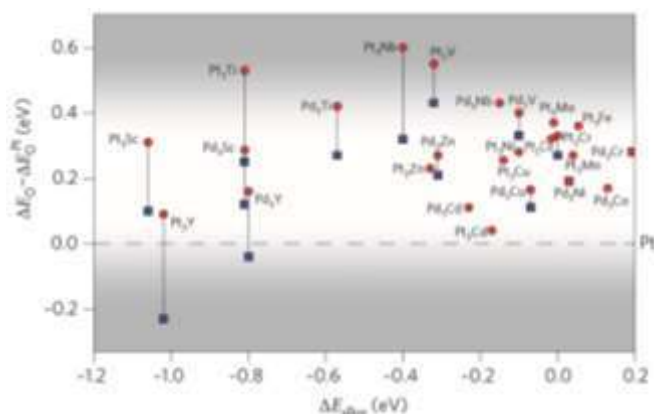
revealed a significant improvement of the ORR activity by a factor of 3 to 6 of Pt-REM alloys over pure Pt. In Figure 2a, the $j_{k@0.9V}$ follows the trend $Pt_3Y > Pt_5Y \approx Pt_5La >> Pt_3Sc > Pt_3Hf > Pt \approx Pt_3Zr \approx Pt_2Y$. The low activity of Pt_3Zr and Pt_3Hf is ascribed to the formation of ZrO_x and HfO_x at the catalyst surface.[17]

Figure 1. DFT calculated oxygen binding energy (relative to Pt) as a function of the alloying energy. The red circles indicate a 50 % of the alloying metal on the second layer, while the blue squares indicate a 25 % of the alloying metal on the second layer. The grayscale gradient indicates the optimal oxygen adsorption for the ORR process. Reproduced with permission from ref [11]. Copyright 2022, Springer.

Based on the relationship derived from theoretical calculations shown in Figure 1, it was predicted that the Pt_3Y and Pt_3Sc alloys would be the most stable among the Pt-REM alloys. The authors rationalized the predicted high stability of Pt-REM alloys by the interaction between the d-orbitals of the two metals, which are approximately half-filled. Therefore, the bonding states are filled and the anti-bonding states are empty.[11]

After experimental accelerated stress tests (AST) designed to elucidate the extent of electrocatalyst degradation under ORR conditions, Pt-REM alloys were more stable than pure Pt or Pt-M (late transition metal) alloys, as they retained 90-70 % of their initial activity.[11] This behavior was related to the transport of the less noble alloying metal atoms, from the bulk of the alloy to the surface, involving intermetallic diffusion energy barrier partially determined by ΔE_{alloy}.[21] This knowledge has provided a framework guiding the investigation and improved understanding of Pt-REM alloys.

3. Pt-REM alloy polycrystalline bulk surfaces

Pioneer contributions from Chorkendorff's group introduced Pt-REM alloys as promising electrocatalysts for the ORR in acidic medium. The research on these electrocatalysts began with the investigation of bulk sputter-cleaned polycrystalline electrodes of Pt_3Y,[11, 17, 22] Pt_5Y,[11, 17, 22] Pt_3Hf,[17] Pt_3Zr,[17] Pt_3Sc,[11, 17] Pt_5Gd,[21a] and Pt_5La.[12] By means of the kinetic current density evaluated at 0.9 V/RHE, $j_{k@0.9V}$, the ORR electrochemical activity of these electrocatalysts was compared, taking as benchmark the polycrystalline Pt surface prepared under the same experimental conditions. As clearly shown in Figure 2a, this comparison
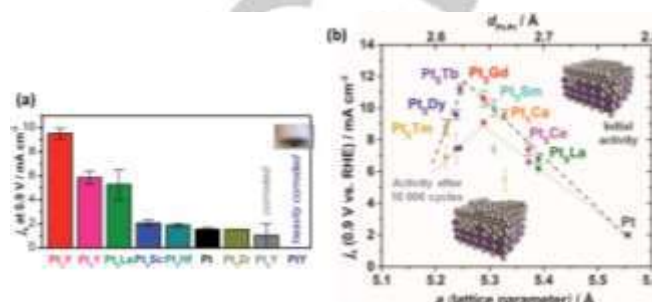

Figure 2 (a) Overall ranking of ORR activity of polycrystalline electrodes of Pt-REM alloys (Reproduced with permission from ref [12]. Copyright 2022, The Royal Society of Chemistry.); and (b) specific activity as function of the bulk lattice parameter (lower axis) and bulk Pt-Pt inter-atomic distance (upper axis). For comparison, it is shown the ORR performance before (darker line) and after (lighter line) the stability test (Reproduced with permission from ref [23]. Copyright 2022).

Lindahl *et al.*[22] studied the ORR activity of Pt-Y thin films with various stoichiometries. The electrochemical evaluation revealed that the activity of Pt_3Y was greater than that of Pt_2Y, Pt_5Y and Pt, demonstrating that the optimal Pt:Y ratio was 3:1. In addition, the effect of the film thickness, from 20 to 80 nm, was probed: a 27 nm thick Pt_3Y film displayed the highest activity with no significant degradation after 10,000 cycles from 0.6 to 1 V/RHE in 0.1 M $HClO_4$.[22] The high activity of the Pt_3Y system was explained in terms of the formation of a specific structure with a few-atoms-thick Pt overlayer and low yttrium content in the second atomic layer.[11] However, owing to the fact that the Y atom radius is bigger than the Pt atom radius, it is expected that the alloy might be under tensile strain, thus the surface will bind the ORR intermediates more strongly than a pure Pt surface, *i.e.* the opposite effect from that required to boost the ORR. Thus, it was also proposed that the ligand effect derived from the yttrium located at the sub-surface counterbalances the tensile strain imposed on the surface Pt atoms.[24]

In further investigation of the activity of Pt-REM alloys, Escudero-Escribano *et al.*[23] have systematically evaluated the ORR activity of a series of sputter-cleaned polycrystalline Pt_5REM electrodes. The observed activity trend was: $Pt_5Tb > Pt_5Gd \approx Pt_3Y > Pt_5Sm > Pt_5Ca \approx Pt_5Dy > Pt_5Tm > Pt_5Ce > Pt_5Y \approx Pt_5La >> Pt$. From structural characterization, it was seen that the lattice parameter and thus the Pt-Pt interatomic distance decrease in the alloys from left to right in the lanthanide series. Based on this feature, a volcano-like plot was built, from where the ORR activity, expressed in terms of j_k, behaves as a function of the lattice parameter of the alloy and, therefore, of the Pt-Pt interatomic distance, see Figure 2b. The authors concluded that the Pt_5REM alloys form an unusual $CaCu_5$–type structure that accommodates the alloying atoms with different radii in a different way from that in FCC and HCP alloys. Despite the bigger atomic radii of REM

4

REVIEW

(with respect to Pt), the closest Pt-Pt nearest neighbor distance is shorter than that in pure Pt,[23] revealing that the electrode is under compressive strain. DFT screenings suggest that a 3-4 atom thick Pt overlayer is formed on the Pt₅REM alloy, the structure of which forms the so-called *kagome* layer.[23] This overlayer is equivalent to a compressed closely packed pure Pt overlayer. [21a]

According to the Sabatier principle, the alloys located on the left-side of the volcano plot in Figure 2b bind OH too weakly, while those on the right-side bind OH too strongly.[23] From this graphic, Pt₅Tb and Pt₅Gd emerge as the most active electrocatalysts for the ORR since, for instance, Pt₅Tb is located at the top of the volcano plot, exhibiting the optimum OH binding energy, thus the highest ORR activity with a lattice compression of *ca.* 3 %. However, this activity was not retained after 10,000 potentiodynamic cycles (from 0.6 to 1.0 V/RHE in 0.1 M HClO₄), which indicates the poor stability of this Pt-REM alloy in the investigated voltage window. In contrast, Pt₅Gd was more stable under the same conditions, which was ascribed to its ΔE_{alloy} of −3.9 eV.[21a] Owing the fact that the standard Gibbs free energy of dissolution ($\Delta G°_{dis}$) of Gd is −7.2 eV (*i.e.* −2.4 V/NHE) and the ΔE_{alloy} of Pt₅Gd stabilizes each Gd atom by −3.9 eV, the standard Gibbs free energy of Pt₅Gd dissolution ($\Delta G°_{dis\ alloy} = \Delta G°_{dis} − \Delta E_{alloy}$) is −3.3 eV, corresponding to −1.1 V/NHE.[21a] Based on this thermodynamic analysis, at 1 V/NHE (conventional open circuit potential for Pt-based ORR electrocatalysts), there is a gap of 2.1 V, promoting a thermodynamic dissolution driving force of −6.3 eV for each Gd atom.[21a] Indeed, the thermodynamic dissolution driving force for other Pt-REM alloys are of the same order of magnitude, giving an explanation for REM dissolution in this system.[12]

Experimental evidence, however, reveals that the formation of the Pt-rich overlayer provides kinetic stability against REM dissolution from the alloy bulk.[18, 21a] As an example, the angle resolved XPS spectra obtained before and after the first ORR evaluation in 0.1 M HClO₄ of bulk polycrystalline Pt₅Gd is depicted in Figure 3.[21a]
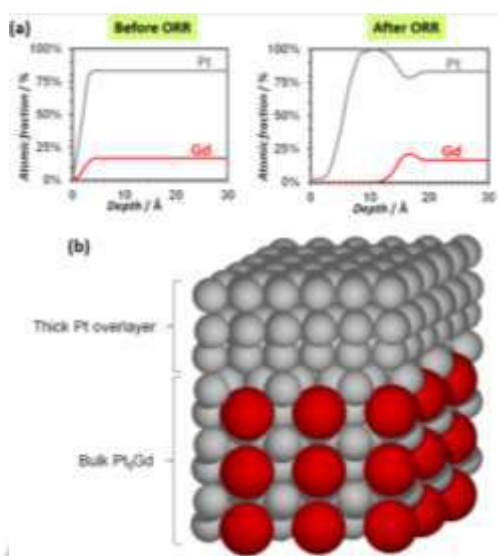

Figure 3. (a) Angle resolved XPS profiles before and after the ORR measurements; and (b) 3D schematization of the Pt₅Gd structure (Pt = gray spheres, Gd = red spheres). Reproduced with permission from ref [21a]. Copyright 2022, American Chemistry Society.

After the electrochemical evaluation in the acidic electrolyte, a compressive strained Pt-rich overlayer formed on Pt₅Gd, which suggests that Gd atoms diffuse from the alloy core towards the surface. Nevertheless, the kinetic barrier for the diffusion of solute metal is primarily determined by ΔE_{alloy} which, for REM, is higher than that of late transition metals,[11] see Figure 1. The origin of the Pt-rich overlayer was explained by two possible phenomena.[12, 21a] The Pt atoms located at the second surface layer can exchange with the REM atoms located at the first surface layer, so increasing the stoichiometry of REM by *ca.* 25-50 % in the second layer.[25] Further, DFT calculations suggest a weakening of the adsorption energy of the oxygen species *via* the induced compressive contraction generated through the interaction between Pt and REM atoms.[12, 21a] Otherwise, the Pt-rich overlayer could originate directly from the REM dissolution from the first surface layer.

From the above discussion, it is clear that the contraction caused by the REM atoms could modulate the strain-effects of the alloy, thus tuning the electrocatalyst ORR activity and stability.[21a, 23] Further DFT calculations suggest that the strain effects might only weaken the OH adsorption energy at the surface[26] (to a certain extent). The weakening of the adsorption energy of other ORR intermediates can be tuned by other phenomena, *e.g.* through the ligand effect.[24]

Despite the high activity driven by Pt-REM bulk polycrystalline surfaces, they cannot be implemented in a fuel cell cathode due to the afforded poor dispersion of active sites. Conventionally, the ORR specific activity represents the electrocatalytic faradic current per electrochemically accessible active site (normalized either by Pt mass or Pt surface). In this sense, the electrochemical active surface area (ECSA) magnitude reflects the Pt utilization with the minimal metal loading.[27] In order to maximize the surface/volume ratio and increase the active sites density per unit mass of Pt, the design of highly dispersed Pt-REM nanoparticles (NPs) is an important target.

4. Pt-REM alloy nanostructures

As for bulk polycrystalline surfaces, sophisticated physical-deposition approaches have been adopted to produce and study Pt-REM at the nanoscale. Hernandez-Fernandez *et al.*,[28] prepared model size-selected NPs of Pt$_x$Y by the magnetron sputter gas aggregation method and characterized their ORR electrocatalytic activity. This physical deposition technique is useful for the synthesis of metallic NPs of materials with high affinity for oxygen (*e.g.* REM). Due to the used ultra-high vacuum conditions, the oxygen concentration is negligible, promoting the formation of the metallic phase rather than the oxide states.

From this study, the authors rationalized the variation of the ORR activity with the particle size of Pt$_x$Y alloys. It was found that the highest mass activity (3.05 A mg$_{Pt}$⁻¹ at 0.9 V/RHE) was reached when the particle size was *ca.* 9 nm diameter, which is higher than that of the Pt benchmark (0.55 A mg$_{Pt}$⁻¹ at 0.9 V/RHE). Through an AST (9,000 cycles between 0.6 and 1 V/RHE in 0.1 M HClO₄ electrolyte), the best Pt$_x$Y catalyst under study retained 63 % of its initial activity. To better understand this result, the structure and

REVIEW

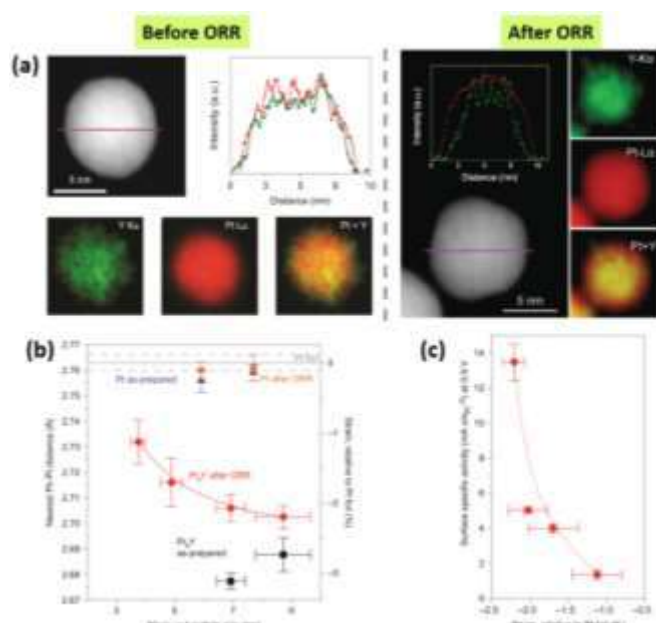morphology of the material was characterized before and after the ORR, *cf.* Figure 4.

Figure 4 (a) STEM micrographs and elemental analysis (EDS) mapping before and after the AST of 9 nm Pt_xY; (b) average nearest-neighbor Pt-Pt distance as a function of the particle size; and (c) surface specific activity as function of the average compressive strain in the Pt_xY particles relative to bulk Pt. (Reproduced with permission.[28] Copyright 2021, Springer).

STEM-EDX analyses provided evidence for a homogeneous distribution of Pt and Y in the as-prepared electrocatalyst. After the ORR, the formation of a Pt-rich shell around the NPs was observed, *cf.* Figure 4a. Accordingly, the Pt:Y surface ratio determined by XPS before the ORR (*ca.* 4) increased after the electrochemical AST characterization (14.3). These results are ascribed to yttrium dissolution during the ORR process.[29] Indeed, theoretical calculations *via* DFT pointed out that the ORR activity of model Pt_3Y should depend on the high concentration of Y atoms at the second surface layer.[11] Succeeding theoretical investigation inferred that the high-activity sites of Pt_3Y and Pt_5Y models are surrounded by Pt atoms, which form a overlayer of thickness 3-4 monolayers.[21b]

Moreover, as already demonstrated for extended surfaces, the Pt-Pt distance in Pt-Y NPs influences the electrochemical performance (Figure 4c). Pt_xY catalysts not only exhibited a lower Pt-Pt distance than that in pure Pt, but also maintained this compressive strain after the ORR measurements. The lattice compression of the Pt_xY structure depends on the particle size, varying from a strain of −1.0 % for 4 nm Pt_xY NPs to −2.1 % for 9 nm Pt_xY NPs, Figure 4b. The enhanced activity derived from the strain effect was linked to a weakening on the OH adsorption energy.[28] The same size-selected NPs model was successfully translated to Pt_xGd alloys,[30] reported as being more active and more stable than Pt_xY NPs. The highest mass activity of Pt_xY and Pt_xGd *ca.* 8-9 nm NPs was explained by means of the strained structure and the optimum surface/bulk ratio,[30] see Figure 4. This particle-size dependent behavior has been observed also for Pt_5Ce/C, with an optimal ORR activity at 8.8 nm.[31]

Furthermore, Malacrida *et al.*[29] followed the dealloying process of Pt_xY NPs (prepared by magnetron sputter gas aggregation method) *in situ* through progressive operation in the presence of oxygen, using *operando* near-ambient pressure XPS analysis. They observed that yttrium oxidation occurred with segregation of Y atoms at the NP surface. The content of metallic Y at the surface decreased substantially as the electrocatalyst was exposed to consecutive oxidative and reductive conditions. Therefore, an Y oxide/hydroxide intermediate was formed on the electrocatalyst surface during operation, followed by its dissolution and the release of Y^{3+} cations into the electrolyte,[29] and leading to the formation of Pt-rich overlayers. The origin and thickness of the Pt overlayer is related to the surface diffusion though the potential cycling,[26] where the REM atoms are transported from the bulk of the alloy to the surface, following their eventual dissolution or oxidation.[21b] This process, indeed, implies an energy barrier which partially depends on the ΔE_{alloy}.[11, 21b]

Although physical deposition techniques (*e.g.* magnetron sputtering gas segregation [28-29, 32]) successfully produce Pt-REM NPs, technological limitations avoid larger scale production (*e.g.* slow deposition rate, limited production to a few micro or nanograms, complexity of the required infrastructure, ultra-high vacuum conditions, and so on),[33] which hinders their implementation in single fuel cells and applicability in PEMFC. Therefore, more practical and scalable chemical synthesis approaches to produce Pt-REM NPs are highly desirable.

Despite much research effort in the last years, the wide range of standard redox potential of REM and their high oxophilicity (favorable to formation of REM oxygen-containing species instead of alloys) are the main stumbling blocks for the chemical synthesis of Pt-REM NPs and their upscale.[21b, 31] So far, for the majority of the chemically-prepared materials reported, there is no irrefutable evidence of alloy formation, *i.e.* the structure consists mainly of REM (hydr)oxide-decorated Pt, forming a Pt/REM-oxide junction.[10b] Since the focus of this work is on Pt-REM alloys, such materials are not discussed here. If the reader is interested in these kinds of materials, we encourage to consult the work of Peera *et al.*[10b].

Recent promising synthesis approaches such as the arc-melting method,[34] impregnation of an REM halide onto a Pt/C catalyst at high temperature treatment under hydrogen,[33, 35] tri-alkyl-borohydride molten salt reducing reaction,[36] carbodiimide-complex route,[31] *etc* have successfully produced Pt-REM alloy nanostructures. In particular, the carbodiimide-complex route[31] is an approach that has attracted particular attention by its simplicity and propensity to scale-up to produce carbon supported Pt-REM NPs. This method is based on the formation of a C-N network with atomically coordinated Pt and REM ions, which upon reduction collapses to rare earth carbodiimide complexes ($REM_2(CN_2)_3$) along with Pt particles and finally leads to Pt-REM nanoalloys. Following this novel route, carbon supported Pt_5Ce, Pt_3Y, Pt_5La, Pt_2Sm, Pt_2Gd and Pt_2Tb alloys were prepared.[31]

Using the carbon supported Pt-Gd nanoalloys as model, the optimal Pt:Gd ratio for high ORR activity was found.[37] By means of a systematic variation of the Gd precursor amount through the carbodiimide-complex route, the Pt:Gd ratio was varied, and it was observed that this parameter influences the crystalline

6

REVIEW

structure, particle size, morphology and near-surface composition of the NPs. As the Pt.Gd ratio increases, an evolution from pure Pt to Pt_2Gd alloy was observed. However, the bulk and the near-surface compositions indicate a Pt-enrichment respect to the formed Pt_2Gd crystalline phase, especially at the near-surface region. This trend is related to the selective dissolution of Gd at the surface during the acidic wash step. This process proceeds until a protective Pt-rich overlayer is formed, stabilizing the particle. Electron microscopy and XPS analyses revealed the presence of two different alloyed structures, the relative amounts of which depend on the Pt:Gd ratio: solid NPs with size < 10 nm, which tend to form a core-shell structure (the alloyed Pt-Gd core is surrounded by Pt overlayers), and particle sizes > 10 nm, which favor the formation of porous nanoarchitectures. The latter are characterized by the presence of cavities that penetrate the entire particle and the presence of some gadolinium oxide, see Figure 5a. Such porous nanoarchitectures predominate at high Gd content. The ORR activity trend revealed a volcano-like curve, *cf.* Figure 5b, with the optimal Pt:Gd ratio at 4.7, achieving NPs of *ca.* 8 nm. Meanwhile, the porous nanoarchitectures display poor ORR activity and stability.[37]
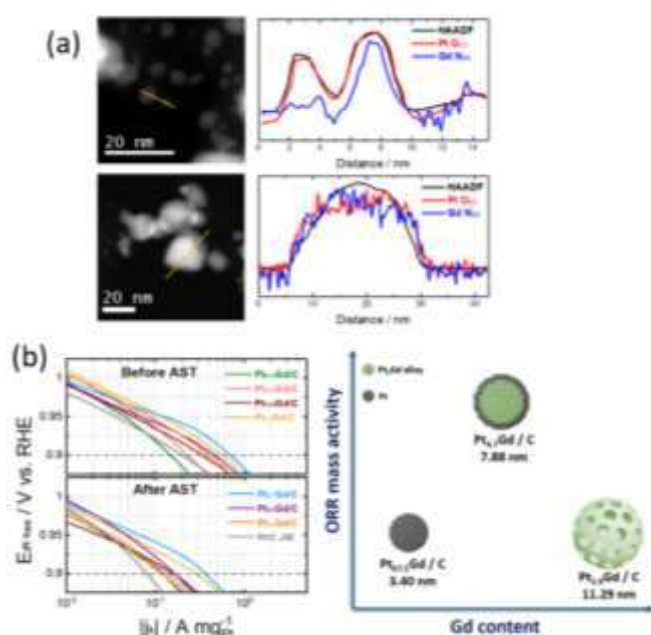

Figure 5 (a) STEM micrographs and the corresponding EELS linear profile of solid NPs and porous nanoarchitectures; and (b) ORR activity ranking of Pt_xGd/C nanostructures. (Reproduced with permission from ref [37] Copyright 2022, American Chemistry Society).

The $Pt_{4.7}Gd/C$ electrocatalyst, however, does not present the expected long-term stability upon AST, mainly due to the poor electrochemical stability of the Pt_2Gd crystalline phase and a mixed population of solid and porous architectures. In fact, the gaseous environment in which the selective dissolution of Gd takes place has a great impact on the free corrosion potential (or open circuit potential, OCP) of a corroding system: the presence of oxygen creates a complex mixed OCP, which affects the selective dealloying kinetics.[38] Under this knowledge, the ORR activity and stability of the $Pt_{4.7}Gd/C$ electrocatalyst were enhanced by minimizing the formation of porous nanostructures through performing the dealloying process under an inert atmosphere.[39]

An effect of the carbon support was observed when developing Pt-Y nanoalloys, whereby the nature and textural properties of the carbon support influences the crystalline phase of the Pt-Y nanoalloy that forms on it, as well as its particle size and near-surface chemistry.[40] Using Ketjenblack EC-300J (KB300) produced almost phase-pure supported Pt_3Y alloy nanoparticles of *ca.* 5 nm size as it is shown in Figure 6a-b. Carbon supports with extremely high surface area, *e.g.* Ketjenblack EC-600JD, lead instead to the formation of small NPs with a low alloying degree, while, carbon supports with lower surface area, *e.g.,* carbon Vulcan XC-72, allow the formation of Pt_3Y and Pt_5Y NPs. Such property transitions, driven by the carbon support, modulate the ORR activity/stability of the nanostructured system, and lead to the best overall performance on $Pt_xY/KB300$ as depicted in Figure 6c.
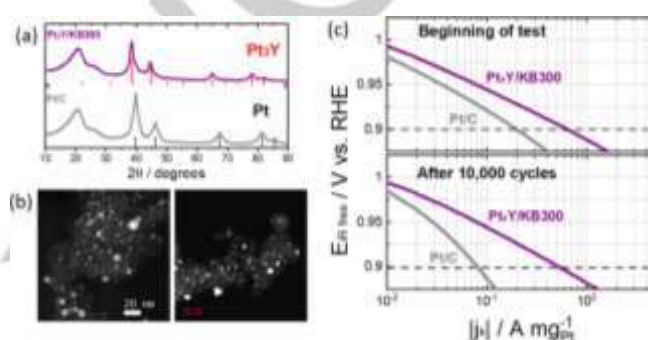

Figure 6 (a) XRD patterns; (b) STEM micrographs; and (c) ORR polarization curves of PtxY/KB300. Commercial Pt/C is used as reference in (a) and (c). (Reproduced with permission from ref [40] Copyright 2022, American Chemistry Society).

Other Pt-REM/C systems at the nanoscale, such as Pt_xLa/C[41] and Pt_xCe/C,[31] have been recently evaluated for the ORR in acidic medium. In both cases, the XRD patterns indicated the formation of a Pt_5REM alloy. Besides, the NPs produced comprise the Pt-REM alloy surrounded by a Pt-rich shell, with higher ORR activity and stability than the Pt/C reference material. An example is given by Itahara *et al.*[35b] at the Toyota Central R&D Labs, Japan, who have synthesized Pt_5Ce/C electrocatalysts using a top-down approach: $CeCl_3$ was impregnated onto commercial Pt/C (Tanaka, 28.7%*wt.* Pt)by heat-treatment at 850 °C for 2 h under $Ar/4\%H_2$ atmosphere. The Pt_5Ce/C electrocatalyst showed higher ORR activity respect to the Pt/C benchmark. Using this method, the authors have produced Pt_5La, Pt_5Sm, Pt-Gd (Pt_5Gd and Pt_2Gd), and Pt_3Tb nanoparticles as well. This contribution evokes the industrial interest on Pt-REM/C electrocatalysts for the ORR.

Table 1 and Figure 7 summarize some of the more relevant data reported so far for Pt-REM alloys (morphology, synthesis route, ECSA, ORR activity and stability in acidic medium). It is evident that Pt-REM at the nanodivided scale improves the ECSA value compared to extended crystalline surfaces by orders of magnitude. Notwithstanding, the ECSA and ORR activity values are still lower than those of other Pt-based electrocatalysts,[42] such as nanowires, shape-controlled alloyed nanostructures, nanoframes, nanoplates, *etc.* Therefore, in spite of the recent advances on the synthesis of carbon-supported Pt-REM NPs, the control of the properties that govern the structure-activity-stability relationships still represents a crucial challenge. For instance, due to the solid-state synthesis approaches, the particle size control

7

and its dispersity are still not satisfactory, and this affects the ECSA values. Another important structural parameter that must be controlled in the Pt-REM nanoalloys is the crystalline phase, since, as is shown in polycrystalline bulk surfaces, the hexagonal Pt_5REM phase provides the best activity/stability values. Thus,

targeting carbon supported Pt-REM NPs with Pt_5REM crystalline phases and highly dispersed nanostructures of 8-9 nm could provide satisfactory high ECSA and ORR activity/stability. Nonetheless, this task is still a current challenge that should be tackled.

Table 1. Summarized synthesis approaches, physicochemical properties and kinetic parameters (electrochemical active surface area, ECSA; specific-surface activity, Is; mass activity, Im) of Pt-REM alloys discussed in this work.

| Electrocatalyst	Size and morphology	ECSA $(m^2\,g_{Pt}^{-1})$	Is@0.9 V/RHE $(mA\,cm_{Pt}^{-2})$	Im@0.9 V/RHE $(A\,mg_{Pt}^{-1})$	Remarks on AST	Ref
Pt_3Y and Pt_3Sc	Polycrystalline disk ($0.196\,cm^{-2}_{geo}$)	$0.20\,cm^{-2}$ (Cu stripping)	6x Pt and 1.5x Pt	n.a.	Transport of Y or Sc atoms from the interior of the alloy to the surface, where they may eventually dissolve or oxidize, will involve an energy barrier determined in part by the heat of formation of the compound.	[11]
Pt_5Ce and Pt_5La	Polycrystalline disk ($0.196\,cm^{-2}_{geo}$)	$0.71\,cm^{-2}$ (CO stripping)	7.40 and 6.80 (geo. area)	n.a.	After 10,000 cycles between 0.6 and 1 V/RHE, Pt_5Ce and Pt_5La catalysts lost 10% and 8% of its initial activity, respectively.	[21b]
Pt_5Gd	Polycrystalline disk ($0.196\,cm^{-2}_{geo}$)	n/a	10.40 (geo. area)	n/a	After 10,000 cycles (0.6-1.0 V/RHE) the percentage of activity loss is 14 %. Most of this loss activity occurring in the first 2000 cycles.	[21a]
Pt_3La	Polycrystalline thin film (thickness of *ca.*213 nm)	$0.20\,cm^{-2}$ (CO stripping)	7.30	n/a	After 3,000 cycles between 0.6 and 1.1 V/RHE, the catalyst retained almost of its initial activity.	[18]
Pt_xY	Unsupported NPs (9 nm)	24 (CO stripping)	13	3.05	After 9,000 cycles between 0.6 and 1 V/RHE, the catalyst retained 63 % of its initial activity, wherein most of the activity losses occur during the first 600 cycles.	[28]
Pt_xGd	Unsupported NPs (8 nm)	44 (CO stripping)	8.20	3.60	After 10,000 cycles between 0.6 and 1 V/RHE, the catalyst retained 70% of its initial activity, wherein most of the activity losses occur during the first 1000 cycles.	[30]
Pt_5Ce/C	Carbon supported NPs (8.8 nm)	60 (CO stripping)	3.95	*ca.*0.70	After 10000 cycles between 0.6 and 1 V/RHE, the catalysts retained *ca.*85% of its initial activity.	[31]
Pt_xGd/C	Carbon supported NPs (7.8 nm)	52 (CO stripping)	1.30	0.68	After 10000 cycles between 0.6 and 0.925 V/RHE, the catalysts retained *ca.*53% of its initial mass activity.	[37]
Pt_xGd/C	Carbon supported NPs (7.6 nm)	38 (CO stripping)	1.96	0.72	After 10000 cycles between 0.6 and 0.925 V/RHE, the catalysts retained *ca.*81% of its initial mass activity.	[39]
$Pt_xY/KB300$	Carbon supported NPs (5.2 nm)	61 (CO stripping)	1.01	0.62	After 10000 cycles between 0.6 and 0.925 V/RHE, the catalysts retained *ca.*82% of its initial mass activity.	[40]
Pt_5La/C	Carbon supported NPs (7.8 nm)	21 (H_{upd})	0.53	0.11	After 10000 cycles between 0.6 and 1 V/RHE, the catalysts retained *ca.*50% of its initial mass activity.	[41]
Pt_5Ce/C	Carbon supported NPs (*ca.* 7 nm)	37 (H_{upd})	*ca.* 0.8	*ca.* 0.35	n.a.	[35b]

REVIEW
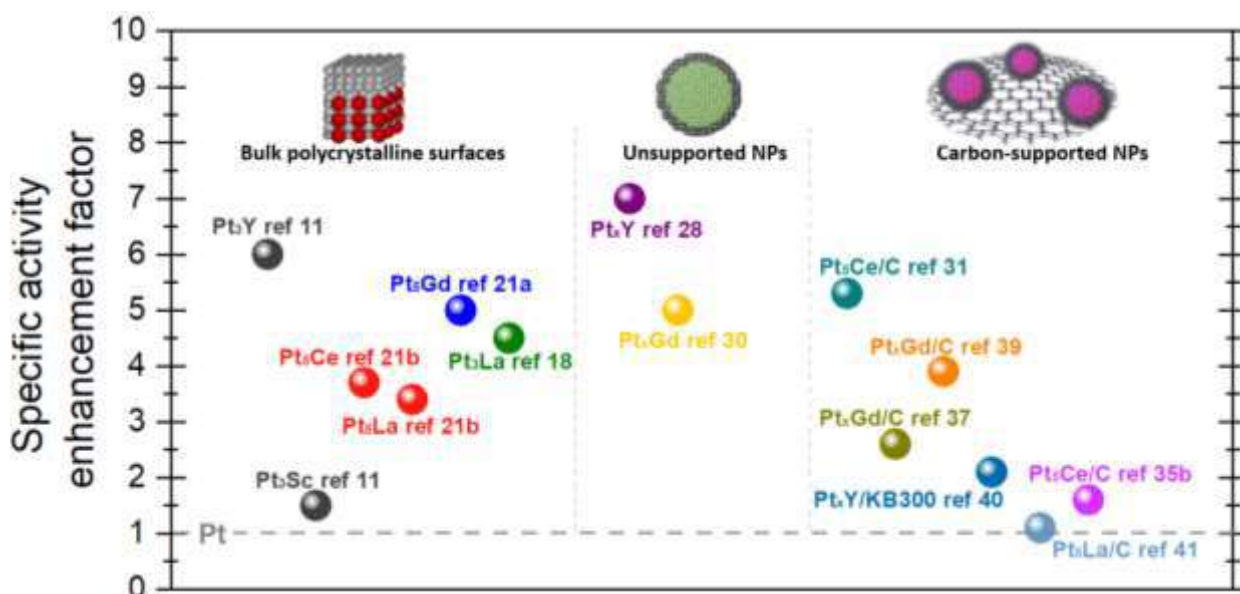
Figure 7 Specific activity enhancement factor, respect to the corresponding reported Pt benchmark material, of Pt-REM alloys discussed in this work.

5. Applications in PEMFC cathodes

So far, few Pt-REM electrocatalysts have been evaluated in a single proton exchange membrane fuel cell. A pioneering contribution is given by Jong Yoo *et al.*, who reported the use of Pt$_x$Y alloys sputter-deposited on a diffusion medium substrate coated with a carbon/ionomer composite layer.[43] By a controlled multilayer sputtering with the application of Nafion-carbon-ink onto the surface (1-layer, 3-layers or 6-layers), the authors showed the impact of mass-loading of the carbon/ionomer composite layer on the PEMFC performance, see Figure 8. The best PEMFC performance was achieved with 3-layers, corresponding to 0.06 mg cm^{-2} of Pt$_3$Y.[43] This electrode presented a higher ORR activity (*ca.* 1000 mA cm^{-2} at 0.6 V) than a pure Pt surface prepared under the same conditions (*ca.* 500 mA cm^{-2} at 0.6 V).[43] Besides, sputter deposited thin films of Pt$_3$Y, Pt$_5$Gd and Pt$_5$Tb were evaluated as cathode electrocatalysts in PEMFC, and an ORR enhancement factor of 2.0-2.5 over pure Pt was observed.[44]

Gasteiger's group has reported a Pt$_x$Y/C electrocatalyst prepared by impregnation of commercial Pt/C with YCl$_3$ and its subsequent heat-treatment under H$_2$ at 1200 °C.[35a] In the half-cell characterization, Pt$_x$Y/C displayed lower ORR activity than commercial Pt/C (210 and 270 A g$_{Pt}^{-1}$, respectively). However, the single fuel cell evaluation revealed that the Pt$_x$Y/C material afforded a significantly enhanced stability during AST (30,000 cycles between 0.6 and 1.0 V), ascribed to the large particle size (*ca.* 10 nm).[35a] Indeed, membrane electrode assembly (MEA) design and measurement optimization still represent issues, which hamper the standardization of results.[35a, 45]
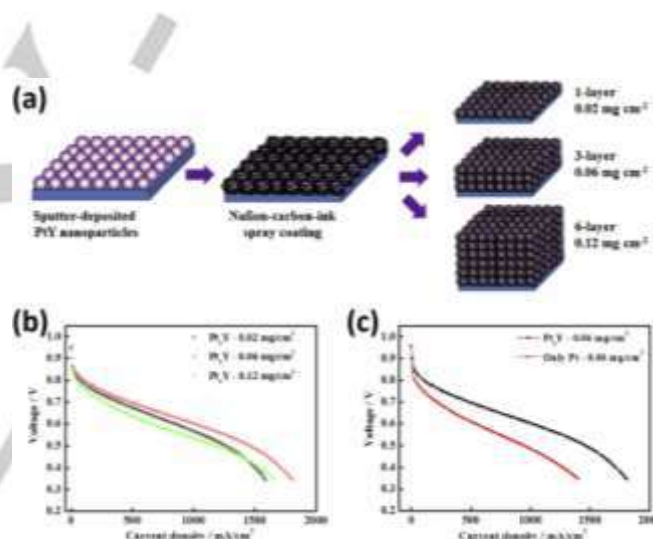

Figure 8 (a) Schematic representation of controlled sputter-deposited Pt$_3$Y nanoparticles; (b) voltage-current curves of Pt$_3$Y as function of deposited layers; and (c) voltage-current curves comparison between optimized Pt$_3$Y and Pt. (Reproduced from ref [43] with permission from Elsevier. Copyright 2022).

Pt$_3$Sm NPs supported on partially exfoliated carbon nanotubes were characterized in PEMFC cathodes.[46] The MEA showed a current density higher than 1000 mA cm^{-2} at 0.6 V and 60 °C, surpassing that of Pt/C (750 mA cm^{-2}) under the same operating conditions. The high ORR activity of Pt$_3$Sm was attributed to a synergistic effect with the exfoliated carbon nanotubes of the support, that led to a lower binding energy of oxygen-containing species than on Pt/C.[46] In Table 2 are reported the results from PEMFC single cell characterization with Pt-REM alloys at the cathode side.

Pt$_x$Gd/C synthetized by the carbodiimide-complex route[37] was characterized in MEA, displaying 1350 mA cm^{-2} at 0.6 V and 80 °C. This performance could be further enhanced by optimizing the ink formulation and the catalyst loading as well as the dealloying conditions. Indeed, as already discussed, the process

9

in inert atmosphere lead to higher ORR activity and stability of the nanoalloys, minimizing the formation of porous nanostructures.[39] However, for the cathode electrocatalyst used in this study, dealloying was performed under air.

Table 2. Summary of Pt-REM alloys performance in PEMFC.

Material	Morphology	Testing conditions	j @0.6 V	Ref
Pt_3Y	Unsupported NPs	Mass-loading of 0.06 mg_{Pt} cm^{-2}. Nafion®112 membrane. Operating temperature of 70 °C. Humidified O_2 and H_2, at stoichiometric ratio of 1.5:2, were introduced at the system at atmosphere pressure.	*ca.*1000 mA cm^{-2}	[43]
Pt_xY/C	Carbon supported NPs	Mass loading of 0.12 mg_{Pt} cm^{-2} Operating temperature of 80 °C. 15 µm membrane (Asahi Kasei Corp., Japan) 5 cm^{-2} cell, differential flow H_2/air polarization curve with an H_2/air flow of 2000/5000 nccm, 100% RH, and 170 kPa abs for both reactants; nccm is defined at standard conditions of 273 K and 101.3 kPa.	*ca.*800 mA cm^{-2}	[35a]
Pt_3Y	Thin films	Nafion®212 membrane. Operating temperature of 80 °C. O_2 and H_2 were both humidified to 100% RH and supplied at 1.5 bar.	40 mA cm^{-2}_{Pt}	[47]
Pt_3Y Pt_5Tb Pt_5Gd	Thin films	Mass loading of *ca*. 0.1 mg_{Pt} cm^{-2}. Nafion®212 membrane. Operating temperature of 80 °C. H_2 and O_2 flows of 14.8 and 7.4 mL min^{-1}.	Pt_3Y: 55 mA cm^{-2}_{Pt} Pt_5Tb: 60 mA cm^{-2}_{Pt} Pt_5Gd: 45 mA cm^{-2}_{Pt}	[44]
Pt_xY/C	Carbon supported NPs	Mass loading of 0.10 mg_{Pt} cm^{-2} Operating temperature of 80 °C. 15 µm membrane (Asahi Kasei Corp., Japan) 5 cm^{-2} cell, differential flow H_2/air polarization curve with an H_2/air flows of 2000/5000 nccm, 95% RH, and 170 kPa abs for both reactants; nccm is defined at standard conditions of 273 K and 101.3 kPa.	*ca.*1290 mA cm^{-2}	[48]
Pt_xGd/C	Carbon supported NPs	Mass loading of 0.1 mg_{Pt} cm^{-2} 15 µm Gore membrane. 50 cm^{-2} cell, operating temperature of 80 °C. 100 kPa, 100/100% RH_{inlet}, H_2/air stoic 2/2	*ca.*1350 mA cm^{-2}	[37] [49]

6. Conclusion and outlook

Pt-REM alloys have emerged as a family of highly active and long-term stable electrocatalysts for potential applications in PEMFC cathodes. Their enhanced ORR activity is related to compressive-strain effects on a Pt overlayer, that weakens the binding energy of the ORR intermediates on the active surface. The observed

10

REVIEW

stability of Pt-REM alloys has been linked to an energy barrier for the diffusion of REM atoms, from the bulk of the alloy to the surface, which depends on the alloy formation energy.

Despite the high mass activity properties of Pt-REM as bulk polycrystalline surfaces, their limited surface/volume ratio and the several drawbacks on their synthesis routes, such as the required synthesis infrastructure, the extremely low produced quantities of catalysts, the slow rate depositions, elevated costs, *etc.* all limit their practical applicability in PEMFC. In this sense, and although the straightforward and up-scalable chemical synthesis of carbon supported Pt-REM nanostructures is highly desirable, it does represent a great challenge, mainly due to the vast standard redox potential and the high oxophillicity of rare earth metals. Many of the "Pt-REM" electrocatalysts presented in the literature are non-alloyed, consisting of Pt/REM oxide junctions, or they were prepared by approaches not leading to the production of supported nanoparticles in a large scale.

Novel and promising chemical routes have been proposed to prepare carbon supported Pt-REM nanoparticles. Such strategies might be adapted and explored in diverse systems with the goal of optimizing the electrocatalytic requirements. Besides, the understanding of these relatively novel systems must be studied in deep to design optimal ORR materials. However, the control of the properties that govern the structure-activity-stability relationships still represents an important challenge. The analysis and comparison between bulk polycrystalline surfaces and recent carbon supported nanoalloys leads to the conclusion that the particle size control, homogeneous particle dispersion, tuning the optimal Pt-REM crystalline phase and the Pt:REM ratio still merit deeper research to implement this family of alloys in PEMFC.

On the other hand, several fundamental questions are still unanswered for this novel nanoalloys. Therefore, new insights must be provided for a better understanding of the behavior of Pt-REM at the nanoscale: *operando* spectroscopic techniques could unravel important information on the degradation mechanisms during the ORR conditions; advanced electron microscopy techniques might be useful to understand the Pt-REM structure before and after the accelerated degradation protocols, *e.g.* the stability of the *kagome* structure and the strain distribution through the particle; DFT screenings would shed light on the structure-activity-stability relationships at the nanoscale, and so on.

Another paramount challenge is the testing in PEMFC, since the study of Pt-REM alloys in MEAs is still quite limited to only a few examples. However, important issues must be addressed, such as the difficulties to prepare sufficiently large quantities of electrocatalyst for the MEA preparation/optimization, the effect of the voltage window in the PEMFC test, the alloy degradation upon voltage-cycling, the problems derived from the testing-system design, the detrimental effect of the metal dissolution on the membrane, *etc.* These drawbacks should be considered in future characterization protocols.

Particularly relevant is achieving/maintaining high MEA performance at high current density values keeping low the Pt loading in the cathode catalyst layer, which requires catalysts displaying high mass activities and high surface areas. However, so far relatively low ECSA values were reported for Pt-REM/C. Therefore, the size of Pt-REM catalyst needs to be the lowest to provide high ECSA, but high enough to present the optimum structure with a compressively strained Pt overlayer (*ca.* 8 nm).

All these considerations lead to the conclusion that the development of chemical up-scalable synthesis approaches allowing the control over size, structure, composition, morphology of Pt-REM nanoparticles is a cutting edge challenge for PEMFC implementation and spreading.

7. Acknowledgements

8. References

[1] I. Staffell, D. Scamman, A. Velazquez Abad, P. Balcombe, P. E. Dodds, P. Ekins, N. Shah, K. R. Ward, *Energy Environ. Sci.* **2019**, *12*, 463-491.

[2] aD. Wu, X. Shen, Y. Pan, L. Yao, Z. Peng, *ChemNanoMat* **2019**, *6*, 32-41; bP. Strasser, S. Kühl, *Nano Energy* **2016**, *29*, 166-177; cN. Alonso-Vante, *Chemphyschem* **2010**, *11*, 2732-2744.

[3] Y. Luo, N. Alonso-Vante, *Electrochim. Acta* **2015**, *179*, 108-118.

[4] G. Ercolano, S. Cavaliere, J. Rozière, D. J. Jones, *Curr Opin Electrochem* **2018**, *9*, 271-277.

[5] aX. Ren, Q. Lv, L. Liu, B. Liu, Y. Wang, A. Liu, G. Wu, *Sustain. Energy Fuels* **2020**, *4*, 15-30; bV. Čolić, A. S. Bandarenka, *ACS Catal.* **2016**, *6*, 5378-5385.

[6] Y. Bing, H. Liu, L. Zhang, D. Ghosh, J. Zhang, *Chem Soc Rev* **2010**, *39*, 2184-2202.

[7] S. Mauger, K. Neyerlin, S. Alia, C. Ngo, S. Babu, K. Hurst, S. Pylypenko, S. Litster, B. Pivovar, *J. Electrochem. Soc.* **2018**, *165*, F238-F245.

[8] G. Ercolano, F. Farina, L. Stievano, D. J. Jones, J. Rozière, S. Cavaliere, *Catal Sci Technol* **2019**, *9*, 6920-6928.

[9] aD. Wang, H. L. Xin, R. Hovden, H. Wang, Y. Yu, D. A. Muller, F. J. DiSalvo, H. D. Abruna, *Nat Mater* **2013**, *12*, 81-87; bS. Kühl, P. Strasser, *Topics in Catalysis* **2016**, *59*, 1628-1637.

[10] aC. W. B. Bezerra, L. Zhang, H. Liu, K. Lee, A. L. B. Marques, E. P. Marques, H. Wang, J. Zhang, *J. Power Sources* **2007**, *173*, 891-908; bS. G. Peera, T. G. Lee, A. K. Sahu, *Sustain. Energ. Fuels* **2019**, *3*, 1866-1891.

[11] J. Greeley, I. E. Stephens, A. S. Bondarenko, T. P. Johansson, H. A. Hansen, T. F. Jaramillo, J. Rossmeisl, I. Chorkendorff, J. K. Norskov, *Nat Chem* **2009**, *1*, 552-556.

[12] I. E. L. Stephens, A. S. Bondarenko, U. Grønbjerg, J. Rossmeisl, I. Chorkendorff, *Energy Environ. Sci.* **2012**, *5*, 6744.

[13] R. Ma, G. Lin, Y. Zhou, Q. Liu, T. Zhang, G. Shan, M. Yang, J. Wang, *Npj Comput Mater* **2019**, *5*, 78-93.

[14] S. Guo, E. Wang, *Nano Today* **2011**, *6*, 240-264.

[15] J. K. Nørskov, J. Rossmeisl, A. Logadottir, L. Lindqvist, *J. Phys. Chem. B* **2004**, *108*, 17886-17892.

[16] V. Tripković, E. Skúlason, S. Siahrostami, J. K. Nørskov, J. Rossmeisl, *Electrochim. Acta* **2010**, *55*, 7975-7981.

[17] I. E. L. Stephens, A. S. Bondarenko, L. Bech, I. Chorkendorff, *ChemCatChem* **2012**, *4*, 341-349.

[18] S. J. Yoo, S. J. Hwang, J.-G. Lee, S.-C. Lee, T.-H. Lim, Y.-E. Sung, A. Wieckowski, S.-K. Kim, *Energ Environ Sci* **2012**, *5*, 7521-7525.

[19] S. Jong Yoo, S. K. Kim, T. Y. Jeon, S. Jun Hwang, J. G. Lee, S. C. Lee, K. S. Lee, Y. H. Cho, Y. E. Sung, T. H. Lim, *Chem Commun* **2011**, *47*, 11414-11416.

[20] D. F. van der Vliet, C. Wang, D. Li, A. P. Paulikas, J. Greeley, R. B. Rankin, D. Strmcnik, D. Tripkovic, N. M. Markovic, V. R. Stamenkovic, *Angew Chem Int Ed Engl* **2012**, *51*, 3139-3142.

[21] aM. Escudero-Escribano, A. Verdaguer-Casadevall, P. Malacrida, U. Gronbjerg, B. P. Knudsen, A. K. Jepsen, J. Rossmeisl, I. E. Stephens, I. Chorkendorff, *J Am Chem Soc* **2012**, *134*, 16476-16479; bP. Malacrida, M. Escudero-Escribano, A. Verdaguer-Casadevall, I. E. L. Stephens, I. Chorkendorff, *J. Mater. Chem. A* **2014**, *2*, 4234-4243.

[22] N. Lindahl, E. Zamburlini, L. Feng, H. Grönbeck, M. Escudero-Escribano, I. E. L. Stephens, I. Chorkendorff, C. Langhammer, B. Wickman, *Adv Mater Interfaces* **2017**, *4*, 1700311.

[23] M. Escudero-Escribano, P. Malacrida, M. Hansen, U. Vej-Hansen, A. Velázquez-Palenzuela, V. Tripkovic, J. Schiøtz, J. Rossmeisl, I. Stephens, I. Chorkendorff, *Science* **2018**, *352*, 73-76.

[24] S. J. Hwang, S. K. Kim, J. G. Lee, S. C. Lee, J. H. Jang, P. Kim, T. H. Lim, Y. E. Sung, S. J. Yoo, *J Am Chem Soc* **2012**, *134*, 19508-19511.

[25] V. R. Stamenkovic, B. S. Mun, M. Arenz, K. J. Mayrhofer, C. A. Lucas, G. Wang, P. N. Ross, N. M. Markovic, *Nat Mater* **2007**, *6*, 241-247.

[26] aA. F. Pedersen, E. T. Ulrikkeholm, M. Escudero-Escribano, T. P. Johansson, P. Malacrida, C. M. Pedersen, M. H. Hansen, K. D. Jensen, J. Rossmeisl, D. Friebel, A. Nilsson, I. Chorkendorff, I. E. L. Stephens, *Nano Energy* **2016**, *29*, 249-260; bE. Zamburlini, K. D. Jensen, I. E. L. Stephens, I. Chorkendorff, M. Escudero-Escribano, *Electrochim Acta* **2017**, *247*, 708-721.

[27] S. Rudi, C. Cui, L. Gan, P. Strasser, *Electrocatalysis* **2014**, *5*, 408-418.

[28] P. Hernandez-Fernandez, F. Masini, D. N. McCarthy, C. E. Strebel, D. Friebel, D. Deiana, P. Malacrida, A. Nierhoff, A. Bodin, A. M. Wise, J. H. Nielsen, T. W. Hansen, A. Nilsson, I. E. Stephens, I. Chorkendorff, *Nat Chem* **2014**, *6*, 732-738.

[29] P. Malacrida, H. Sanchez Casalongue, F. Masinia, S. Kaya, P. Hernández-Fernández, D. Deiana, H. Ogasawara, I. Stephens, A. Nilsson, I. Chorkendorff, *Phys. Chem. Chem. Phys.* **2015**, *17*, 28121-28128.

[30] A. Velázquez-Palenzuela, F. Masini, A. F. Pedersen, M. Escudero-Escribano, D. Deiana, P. Malacrida, T. W. Hansen, D. Friebel, A. Nilsson, I. E. L. Stephens, I. Chorkendorff, *J. Catal.* **2015**, *328*, 297-307.

[31] Y. Hu, J. Jensen, L. Cleemann, B. Brandes, Q. Li, *J. Am. Chem. Soc.* **2020**, *142*, 953-961.

[32] F. Masini, P. Hernandez-Fernandez, D. Deiana, C. E. Strebel, D. N. McCarthy, A. Bodin, P. Malacrida, I. Stephens, I. Chorkendorff, *Phys Chem Chem Phys* **2014**, *16*, 26506-26513.

[33] C. Roy, B. P. Knudsen, C. M. Pedersen, A. Velázquez-Palenzuela, L. H. Christensen, C. D. Damsgaard, I. E. L. Stephens, I. Chorkendorff, *ACS Catal.* **2018**, *8*, 2071-2080.

[34] C. Benndorf, H. Eckert, O. Janka, *Dalton Trans* **2017**, *46*, 1083-1092.

[35] aJ. N. Schwämmlein, G. S. Harzer, P. Pfändner, A. Blankenship, H. A. El-Sayed, H. A. Gasteiger, *J Electrochem Soc* **2018**, *165*, J3173-J3185; bH. Itahara, Y. Takatani, N. Takahashi, S. Kosaka, A. Nagoya, M. Inaba, Y. Kamitaka, Y. Morimoto, *Chemistry of Materials* **2022**, *34*, 422-429.

[36] J. S. Kanady, P. Leidinger, A. Haas, S. Titlbach, S. Schunk, K. Schierle-Arndt, E. J. Crumlin, C. H. Wu, A. P. Alivisatos, *J Am Chem Soc* **2017**, *139*, 5672-5675.

[37] C. A. Campos-Roldán, F. Pailloux, P.-Y. Blanchard, D. J. Jones, J. Rozière, S. Cavaliere, *ACS Catalysis* **2021**, 13519-13529.

[38] L. Gan, M. Heggen, R. O'Malley, B. Theobald, P. Strasser, *Nano Lett* **2013**, *13*, 1131-1138.

[39] C. A. Campos Roldán, F. Pailloux, P.-Y. Blanchard, D. J. Jones, J. Rozière, S. Cavaliere, *Nanoscale Advances* **2021**.

[40] C. A. Campos-Roldán, A. Parnière, N. Donzel, F. Pailloux, P.-Y. Blanchard, D. J. Jones, J. Rozière, S. Cavaliere, *ACS Applied Energy Materials* **2022**, *5*, 3319-3328.

[41] C. Fan, P. Wen, G. Li, G. Li, J. Gu, Q. Li, B. Li, *Journal of Alloys and Compounds* **2022**, *894*, 161892.

[42] M. Escudero-Escribano, K. D. Jensen, A. W. Jensen, *Curr Opin Electrochem* **2018**, *8*, 135-146.

[43] S. J. Yoo, K.-S. Lee, S. J. Hwang, Y.-H. Cho, S.-K. Kim, J. W. Yun, Y.-E. Sung, T.-H. Lim, *Int J Hydrogen Energ* **2012**, *37*, 9758-9765.

[44] B. Eriksson, G. Montserrat-Sisó, R. Brown, T. Skála, R. Wreland Lindström, G. Lindbergh, B. Wickman, C. Lagergren, *Electrochimica Acta* **2021**, *387*, 138454.

[45] R. Sandström, E. Gracia-Espino, G. Hu, A. Shchukarev, J. Ma, T. Wågberg, *Nano Energy* **2018**, *46*, 141-149.

[46] M. S. Garapati, R. Sundara, *Int J Hydrogen Energ* **2019**, *44*, 10951-10963.

[47] N. Lindahl, B. Eriksson, H. Grönbeck, R. W. Lindström, G. Lindbergh, C. Lagergren, B. Wickman, *ChemSusChem* **2018**, *11*, 1438-1445.

[48] P. A. Loichet-Torres, Y. Li, C. Grön, T. Lazaridis, C. Liebscher, P. Watermeyer, H. Gasteiger, *Manuscript in preparation* **2022**.

[49] A. Bonastre Martinez, D. Fongalland, J. A. Sharman, C. A. Campos Roldan, S. Cavaliere, D. J. Jones., in *Unpublished results 2022 in FCH JU IMMORTAL GA 101006641.*, **2022**.

WILEY-VCH

REVIEW

Entry for the Table of Contents
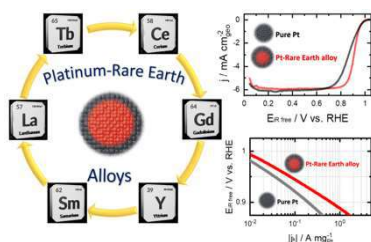
The recent progress on platinum-rare earth alloys for the oxygen reduction reaction, from bulk polycrystalline surfaces to carbon supported nanostructures, is briefly discussed, identifying and establishing the challenges in synthesis and properties design for advanced electrocatalysts for fuel cells.

Institute and/or researcher Twitter usernames: ((optional))